Proceedings of ASME Turbo Expo 2015: Turbine Technical Conference and Exposition
GT2015
June 15 – 19, 2015, Montréal, Canada

GT2015-42727

EXPERIMENTAL RESULTS OF THE FIRST TWO STAGES OF AN ADVANCED TRANSONIC CORE COMPRESSOR UNDER ISOLATED AND MULTI-STAGE CONDITIONS

Patricia S. Prahst
Zin Technologies, Inc
Cleveland, OH USA

Sameer Kulkarni
NASA Glenn Research Center
Cleveland, OH USA

Ki H. Sohn, Ph.D.
The General Electric Company
Cincinnati, OH USA

ABSTRACT

NASA's Environmentally Responsible Aviation (ERA) Program calls for investigation of the technology barriers associated with improved fuel efficiency for large gas turbine engines. Under ERA, the highly loaded core compressor technology program attempts to realize the fuel burn reduction goal by increasing overall pressure ratio of the compressor to increase thermal efficiency of the engine. Study engines with overall pressure ratio of 60 to 70 are now being investigated. This means that the high pressure compressor would have to almost double in pressure ratio while keeping a high level of efficiency.

NASA and GE teamed to address this challenge by testing the first two stages of an advanced GE compressor designed to meet the requirements of a very high pressure ratio core compressor. Previous test experience of a compressor which included these front two stages indicated a performance deficit relative to design intent. Therefore, the current rig was designed to run in 1-stage and 2-stage configurations in two separate tests to assess whether the bow shock of the second rotor interacting with the upstream stage contributed to the unpredicted performance deficit, or if the culprit was due to interaction of rotor 1 and stator 1. Thus, the goal was to fully understand the stage 1 performance under isolated and multi-stage conditions, and additionally to provide a detailed aerodynamic data set for CFD validation. Full use was made of steady and unsteady measurement methods to understand fluid dynamics loss source mechanisms due to rotor shock interaction and endwall losses.

This paper will present the description of the compressor test article and its measured performance and operability, for both the single stage and two stage configurations. We focus the paper on measurements at 97% corrected speed with design intent vane setting angles.

NOMENCLATURE

IGV	Inlet Guide Vane
LE	Leading Edge
Nc	Corrected Speed
OTR	Over-the-rotor
PR	Pressure Ratio
PT	Total Pressure
PS	Static Pressure
R1	Rotor 1
S1	Stator 1
TE	Trailing Edge
TT	Total Temperature

INTRODUCTION

The current work is centered on the development of core compressor front stage technology as an enabler for higher overall pressure ratio to improve engine fuel consumption. Current commercial engines run at overall cycle pressure ratios of 30-45 but study engines are now looking at overall pressure ratios in the 60-70+ range. One key enabler to such high cycle pressure ratios are compressors with significantly higher pressure ratios.

This test program aims to investigate the current technical barriers to highly loaded front stages suitable for a very high pressure ratio compressor. The test program focuses on the front two transonic stages of an experimental GE compressor. Measured performance of this compressor in prior tests did not meet its design intent high speed efficiency goals because of unpredicted losses thought to be in the front two stages of the compressor. These losses were not fully understood and have not been predicted by sophisticated compressor computational fluid dynamics (CFD) simulations, including multi-blade row unsteady CFD of IGV through rotor 2.

The current test was designed to initially run the compressor in a 1-stage configuration to fully characterize and understand stage 1 in isolation. Subsequently, it was run in the 2-stage configuration. This was done to isolate the effect of the bow shock of rotor 2 impinging on the upstream blade rows. Advanced diagnostic instrumentation was put in place for the 2-stage configuration to fully characterize the interaction effects of the rotor 2 upstream traveling shock system on stator 1 and on the wakes from stator 1 and rotor 1. The goal was to fully understand the loss mechanisms, thus permitting the development of highly loaded front stages that mitigate the identified losses and permit the core compressor to reach its target level of efficiency.

TEST COMPRESSOR

The compressor vehicle used in this work includes the first 2 stages of a GE highly loaded axial compressor. The first test consisted of strut, IGV, rotor 1, and stator 1, with a downstream de-swirl vane. The second test consisted of strut, IGV, rotor 1, stator 1, rotor 2, and stator 2 (no de-swirl vane). The IGV, stator 1, and stator 2 are variable geometry and follow a vane schedule that is tied to the speed. Data was acquired at various off-schedule vane angles in order to change loading on the rotors and assess performance, but the focus of this paper is on the nominal vane setting angles.

The test rig was designed to investigate the source of high, unpredicted loss in the compressor. In order to isolate the first stage from any interaction loss effects caused by the downstream stage, the rig has the unique capability to operate in a 1-stage or 2-stage configuration. Figure 1 shows cross-sections of the rig in the respective 1-stage and 2-stage capable configurations.

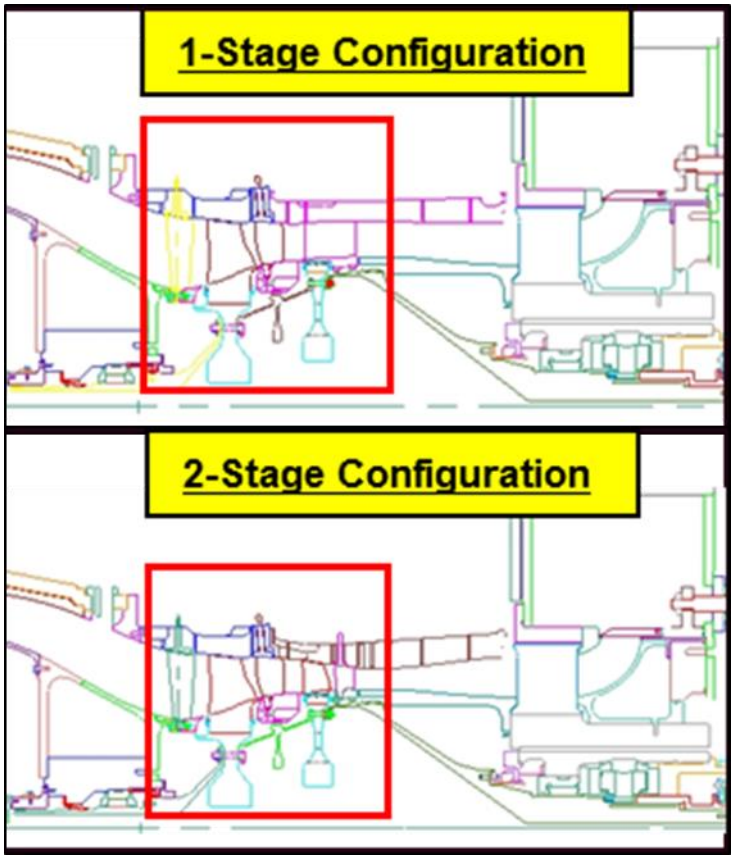

Figure 1. 1-Stage and 2-Stage Rig Configurations

TEST FACILITY

The NASA Glenn Research Center W-7 High Speed Multi-stage Axial Compressor Facility, shown in Figure 2, was used to conduct the testing of the compressor. The facility components supporting this test include a 15,000 hp synchronous drive motor capable of operation between 300 and 3,600 rpm, and a 5.21:1 ratio gearbox resulting in a maximum compressor shaft speed of 18,756 rpm.

Atmospheric air is drawn from the roof of the facility. The air passes through a V-cone flow meter, coarse and fine metering valves, and the plenum tank for flow conditioning prior to entering the test article. Air is exhausted through a collector, and discharged either to an atmospheric vent, to a low vacuum blower (approx. 13 psia), or to the centralized altitude exhaust system (approximately 2 psia vacuum). Maximum altitude exhaust flow is 100 lb_m/s. Vacuum connections are available for boundary layer bleed independent of compressor flow control. Hydraulic controls systems are used for exhaust throttle valve and test article vane actuation. Service air system is used for 0-5 lb_m/s bore flow ambient temperature air supply.

Data acquisition capabilities existing in the test cell include ESP data acquisition system to obtain steady state pressures up to 150 PSIA, Dewetron system for unsteady data acquisition, ESCORT data recording system to obtain and display steady state pressures and temperatures, test parameters, and facility health monitoring data, and Programmable Logic Controller (PLC) for facility control systems.

A GE supplied proprietary data acquisition and probe actuation system was used to actuate traversing probes to obtain 5-hole probe data, dynamic pressures, and hot wire data. Rotor clearances were monitored by a GE proprietary system and read by the NASA ESCORT steady state data acquisition system.

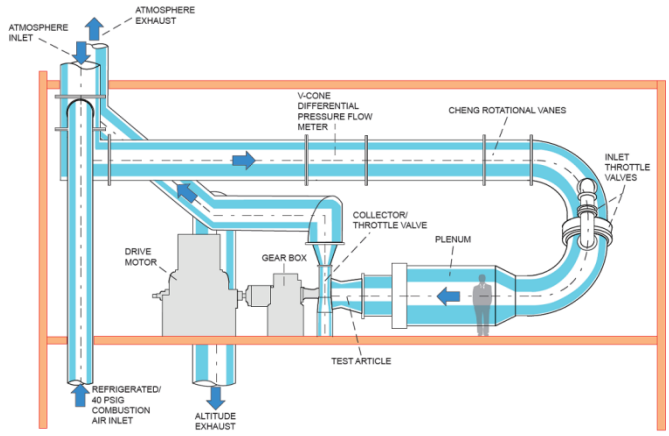

Figure 2. W7 High Speed Multistage Compressor Facility

W-7 Facility Capabilities	
Parameter	**Operating value**
Inlet air pressure	atm to 20 psig
Inlet airflow	100 lb_m/s
Atmospheric exhaust	0.8 psid blowers
Altitude exhaust	26 in. Hg (vacuum)
Rotor speed	18,700 rpm
Rotor size	20 to 22 in.
Drive motor	15,000 hp

Table 1. W-7 Facility Capabilities

TEST PROCEDURE

The single stage compressor test was conducted using steady state instrumentation to obtain performance maps. Most data was acquired at 100% and 97% Nc, but the focus of this paper is on the 97% Nc results only. Figure 3 shows the instrumentation in the rig for the 1-stage test.

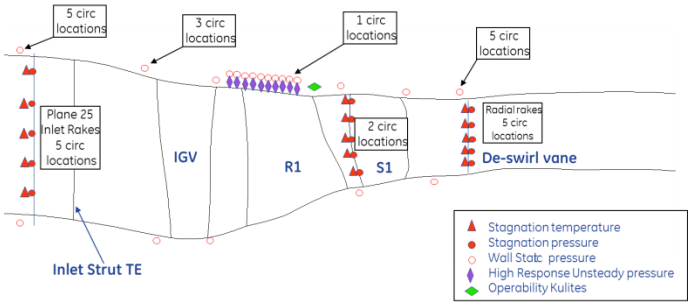

Figure 3. Aero Instrumentation for 1-Stage Configuration

Inlet rakes established the inlet total pressure and temperature profiles. These were located mid-pitch of the strut at 5 circumferential locations, with 5 radial elements located on equal areas. Dynamic static pressure Kulites and steady state static pressure ports were located above the rotor tip to determine rotor start and unstart and to capture rotor shock and tip vortex information. These OTR blocks consist of an axial row of static pressure taps to measure the steady static pressure levels and 2 rows of high response Kulites that are capable of measuring the unsteady pressure over the rotor. Relating the signal

with the rotor passing frequency provides a detailed view of the rotor static pressure field.

To obtain rotor performance, 2 stator vanes were instrumented with total pressure probes along 5 radial locations on the leading edge. An additional 2 stator vanes were instrumented with temperature sensors along 5 radial locations on the leading edge. The overall performance of the stage was measured by 5 circumferentially spaced exit rakes situated downstream of stator 1 at the leading edge of the de-swirl vane. These rakes had total pressure and total temperature sensors at 5 radial locations. The rakes were spaced circumferentially every 20% of stator 1 pitch to capture the stator exit flow. There were a number of casing and hub static pressures all along the flow path from the inlet through the diffuser section.

Overall performance of the 1-stage configuration was measured using the exit rakes referenced to the inlet rakes. Detailed traverse measurements were also made at the exit of the stage and downstream of rotor 1 and stator 1, as shown in Figure 4, to obtain finer data definitions. Rotor 1 performance was measured using the stator 1 leading edge instrumentation

As shown in Figure 4, detailed traverse measurements were made at four locations in the 1-stage configuration: behind the strut, behind the IGV TE, behind rotor 1 TE, and behind stator 1 TE.

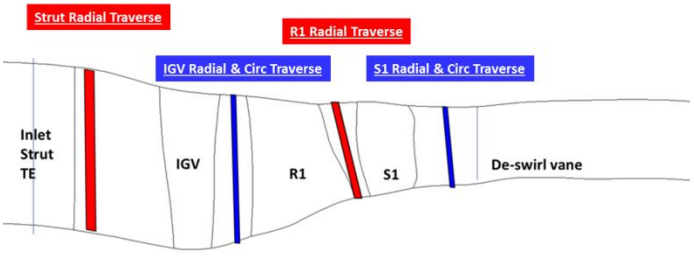

Figure 4. 1-Stage Traversing Instrumentation

The IGV traverse data characterized rotor 1 inflow. This inlet flow field is important to break out losses associated with the inlet ducting system, as typical on-board instrumentation does not pick up losses from the strut, gooseneck, and IGV. This data also identifies rotor 1 inlet boundary conditions for future post-test computations. A 5-hole probe was traversed circumferentially at 8 radial locations across almost two pitches of the IGV to characterize the wakes of the IGV and the inlet strut.

5-hole probe and Kulite radial traverses measured total pressure and total temperature of the rotor 1 exit flow. Radial and circumferential 5-hole probe, Kulite, and X-wire traverses were made at stator 1 TE to measure total and static pressure, total temperature, and 3 components of velocity.

In addition to the previously mentioned instrumentation, the 2-stage configuration included stator 2 leading edge total pressure and total temperature probes and over-rotor dynamic pressure blocks over rotor 2. The exit rakes were moved downstream of stator 2. Figure 5 shows the instrumentation for the 2-stage test.

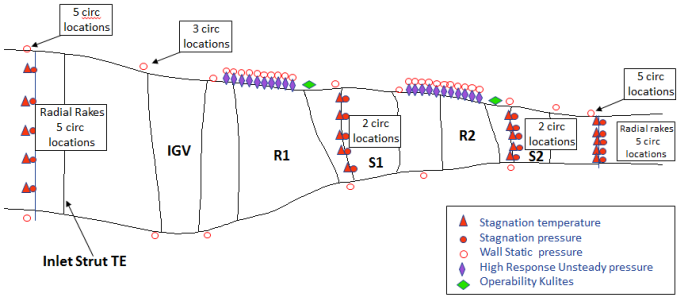

Figure 5. Aero Instrumentation for 2-Stage Configuration

Detailed surveys were also done in the 2-stage configuration with 5-hole probe, Kulites and hot wires. Figure 6 shows the survey locations for the 2-stage configuration. The surveys consisted of the same probes as for the 1-stage configuration. Additional survey locations were included to characterize rotor 2 and stator 2 exit flows.

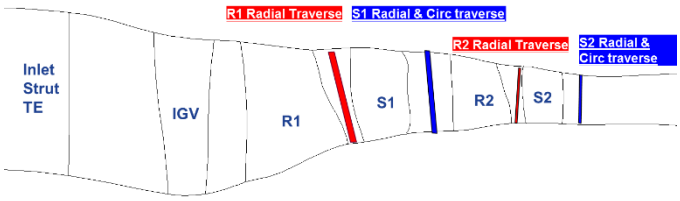

Figure 6. 2-Stage Traversing Instrumentation

The static pressure measurement at the inlet had an accuracy of +/-.015 psi, while at the exit it was +/- 0.03 psi, while the delta temperature measurements had an accuracy of +/- 0.5 R, which results in efficiency uncertainty of +/-.33 points. Based on the V-cone flow

measurement device, the massflow was measured at +/- 1.04% accuracy.

TEST DATA

The 1-stage and 2-stage compressor performance was measured with steady state instrumentation at 97% Nc. This speed was chosen to address the loss issue that was found in prior multi-stage tests conducted by GE. To make comparison between the 1- and 2-stage tests, the conditions for the test were set based on the Stator 1 leading edge instrumentation. We focus on 97% corrected speed to look at the data in more detail.

Figure 7 shows the pressure ratio and adiabatic efficiency as a function of corrected mass flow for the 1-stage configuration.

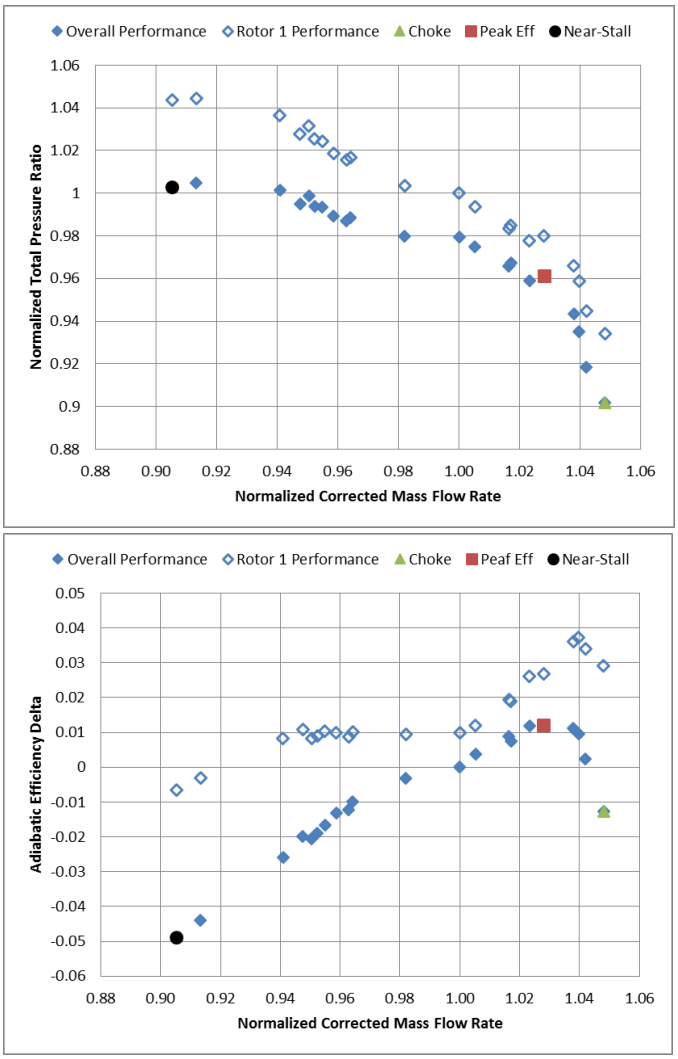

Figure 7. 1-Stage 97% Nc Speedline showing Rotor 1 and Overall Performance

The figure is shown with the overall stage performance (measured by exit rakes) in filled symbols and the rotor performance (measured by stator 1 leading edge probes) in open symbols. The total pressure ratio has been normalized by the operating line total pressure ratio at 97% Nc, and the adiabatic efficiency shown is the delta from the operating line adiabatic efficiency at 97% Nc. The black circle shows the near-stall point, the red square shows the peak efficiency point, and the green triangle shows the choke flow point.

Performance of the 2-stage configuration at 97% Nc is shown in Figure 8. Here, the stage 1+rotor 2 performance (measured by stator 2 leading edge probes) is shown as crosses. The peak efficiency, choke and near-stall points are highlighted. These occur at different

points in the 2-stage configuration as compared to the 1-stage configuration. This is because the second stage choked at a lower flow rate than the first stage.

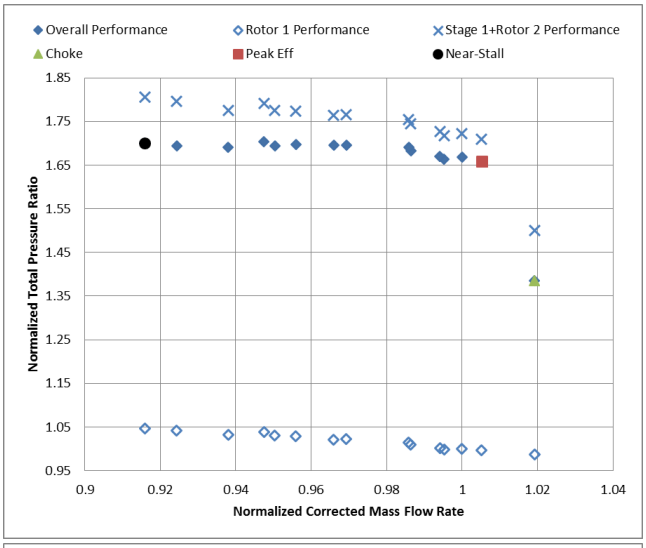

Figure 8. 2-Stage 97% Nc Speedline showing Rotor 1, Rotor 2 and Overall Performance

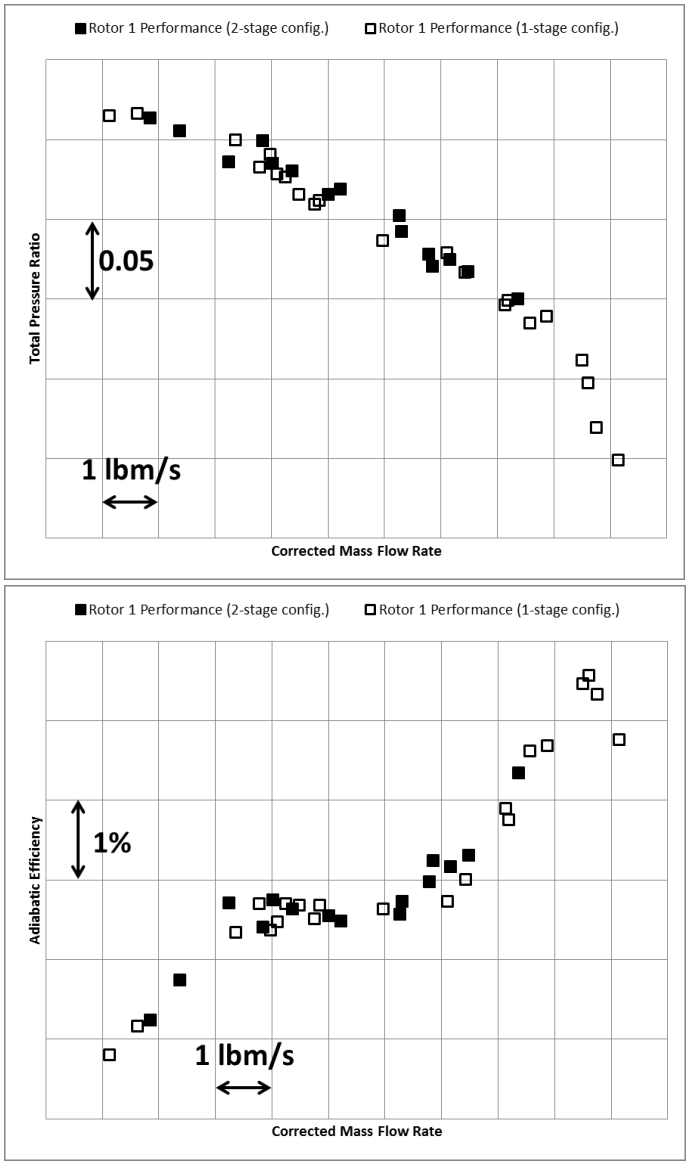

Figure 9. Rotor 1 Performance at 97% Nc in 1-Stage and 2-Stage Configurations

The rotor 1 performance within the 1-stage and 2-stage configurations are compared in Figure 9. The figure indicates that the level of rotor 1 performance is not affected by the presence of the second stage. This is evidence that the rotor 2 bow shock does not have significant impact on the flow near the stator 1 leading edge. Figure 9 also shows that the peak efficiency point in the 1-stage configuration could not be achieved in the 2-stage configuration. That is, rotor 1 cannot operate at its peak efficiency point in the multistage configuration. This is because the second stage choked at a flow rate lower than 1-stage configuration's peak efficiency flow

rate. This points to a mismatch between stages 1 and 2 due to unpredicted losses within the first stage, and rotor 2 bow shock interaction with stage 1 is unlikely to be the phenomenon driving this performance deficit.

DETAILED TEST DATA

The inlet total pressure profile into the IGV is shown in Figure 10. This profile was typical for all run conditions. It is shown here as a ratio to the average plenum total pressure. This profile was generated using an inlet flow conditioning screen to set up the flow field intended for this test. The total temperature profile was flat.

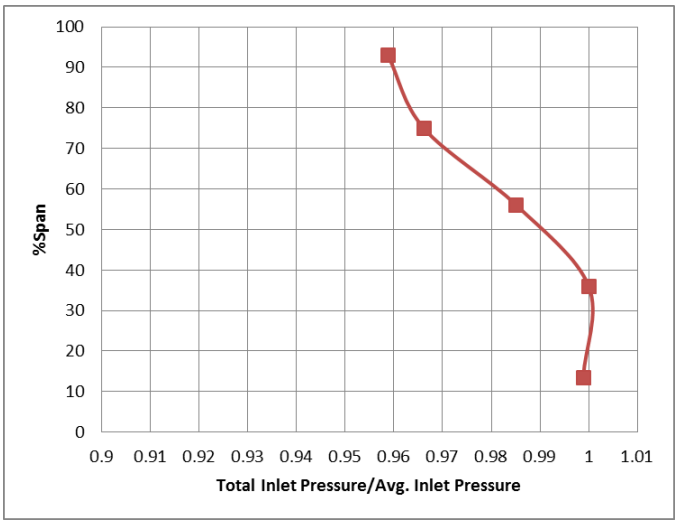

Figure 10. Inlet Total Pressure Profile

A radial-circumferential traversing survey was taken behind the IGV to characterize wakes associated with the IGV and the upstream struts. Figure 11 shows a contour of the total pressure field behind the IGV taken with a 5-hole probe.

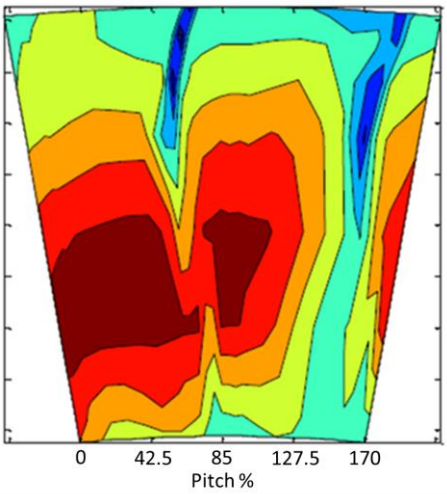

Figure 11. Total Pressure Profile behind the IGV

Figure 11 shows an IGV wake on the left (70% pitch) and an enlarged wake, which is a strut wake combined with an IGV wake, on the right (150% pitch).

Figures 12 and 13 show the total pressure and total temperature profiles, respectively, from the stator 1 leading edge, stator 2 leading edge, and exit rakes from the 1- and 2-stage configurations for the choke, peak efficiency, and near-stall points at 97% Nc. Note that the 1-stage exit rakes are located axially approximately where the stator 2 leading edge probes are located in the 2-stage configuration. The stator 1 leading edge instrumentation is at the same axial location for both configurations.

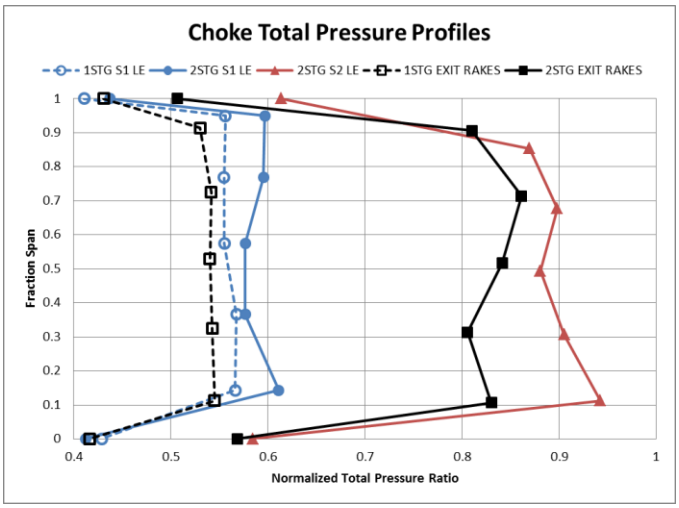

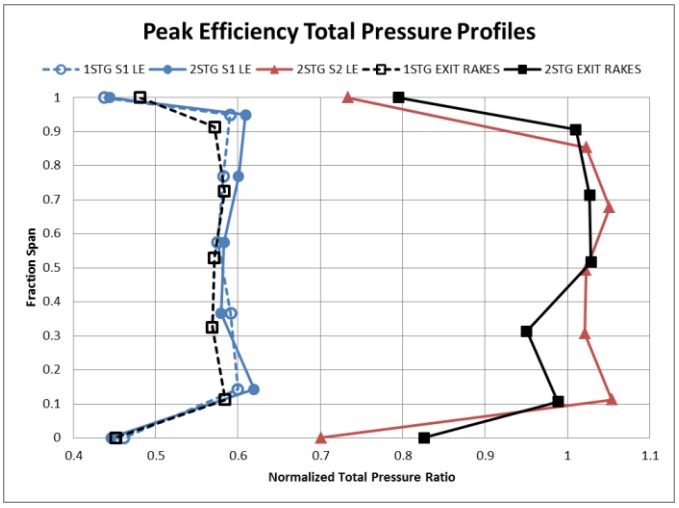

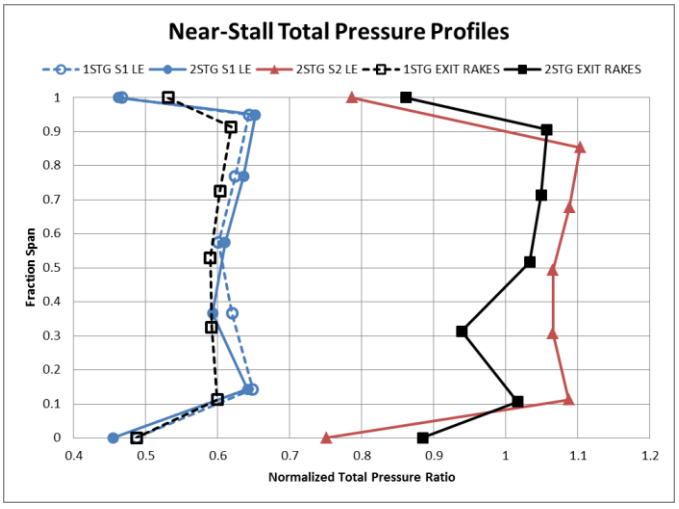

Figure 12. Total Pressure Profiles for Choke, Peak Efficiency, Near-Stall for 1-stage and 2-stage configurations.

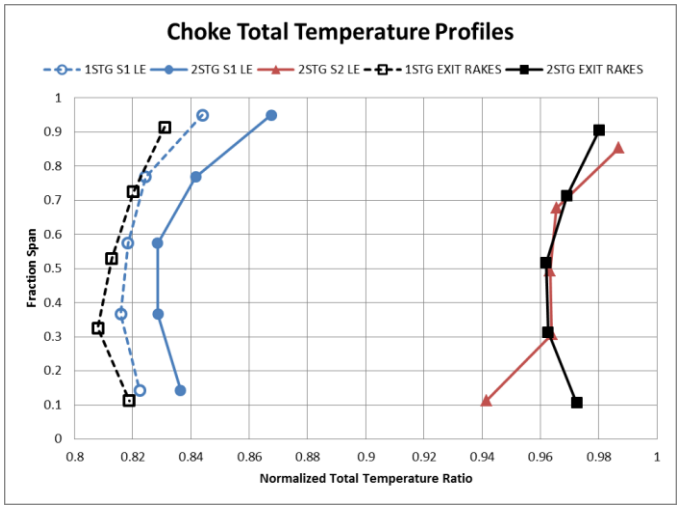

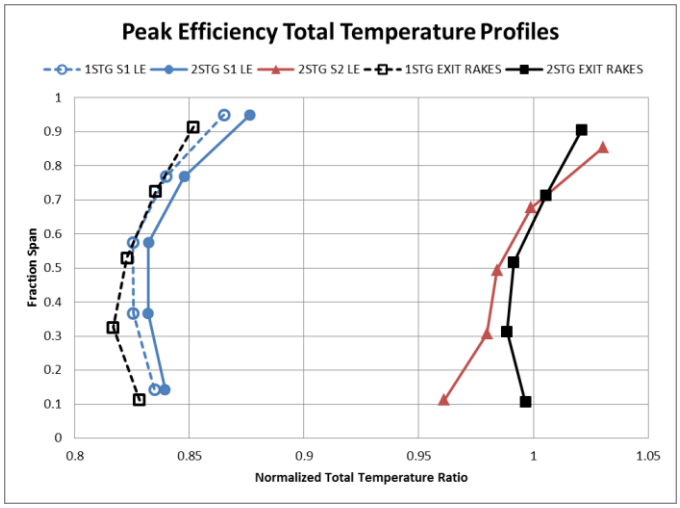

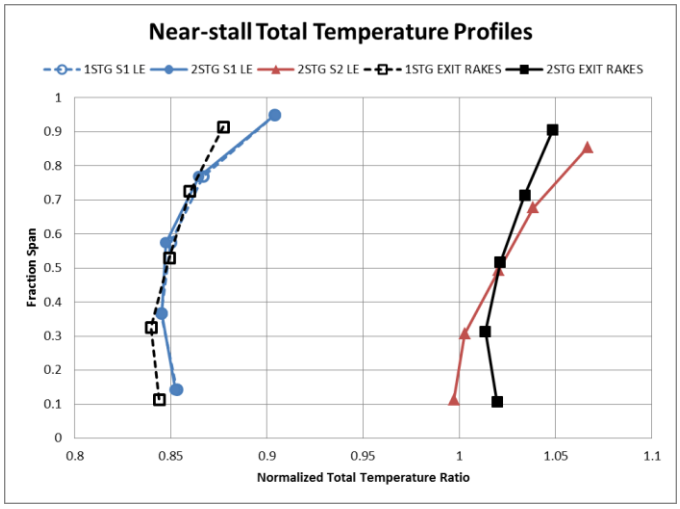

Figure 13. Total Temperature Profiles for Choke, Peak Efficiency, Near-Stall for 1-stage and 2-stage configurations.

The largest differences between the 1-stage and 2-stage configurations are at their relative choked conditions.

Since the second stage chokes at a lower flow rate than the first stage, rotor 1 is throttled to a higher pressure ratio and temperature ratio at the choke point of the 2-stage configuration than it is at the choke point of the 1-stage configuration. This is clearly seen in the choke profiles of stator 1 leading edge probes in Figures 12 and 13 and explains the observed differences. Likewise, but to a lesser degree, the presence of the second stage prevented stage 1 from reaching the 1-stage configuration's peak efficiency point, and so the peak efficiency point of the 2-stage configuration throttles rotor 1 to a higher pressure and temperature ratio than the peak efficiency point of the 1-stage configuration. The near-stall points of two configurations are relatively close in terms of stalling mass flow rate and pressure ratio, so there are relatively smaller differences in stator 1 leading edge measurements between the two configurations.

During 1-stage configuration testing, it was observed that the exit rake total temperature profiles were generally somewhat lower than the stator 1 leading edge profiles. This can be seen in Figures 12 and 13 and is currently postulated to be due to a probe aerodynamic blockage locally throttling rotor 1 to higher loading in a non-axisymmetric way. A hole in total pressure is observed at approximately 30% span of the exit rakes in the 2-stage configuration, which is not seen in the stator 2 leading edge profiles. This may be attributable to stator 2 button tip gap vortex and under-stator 2 platform leakage flow.

Downstream of stator 1, detailed surveys were taken by a 5-hole probe that measured total pressure, total temperature, and absolute flow angle. Figure 14 shows these contours behind stator 1 at the peak efficiency point for the for the 1-stage configuration at the 97% Nc.

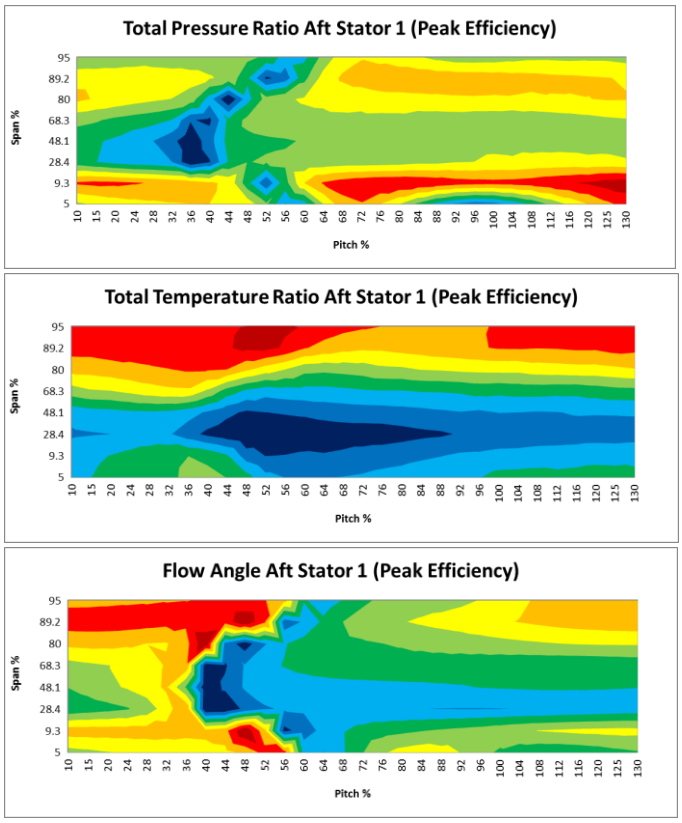

Figure 14. 5-Hole Probe Data at Peak Efficiency Point – Total Pressure, Total Temperature and Flow Angle Contours behind Stator 1 (1-stage configuration).

The data shown in Figure 14 were the result of a circumferential-radial traversing across 120% of stator 1 trailing edge pitch. The stator 1 wake structure is captured in the total pressure and flow angle data between 32% and 56% pitch.

Kulites located over rotor 1 measured the RMS pressure and static pressure at choke, peak efficiency, and near-stall points at 97% Nc for the 1-stage configuration. These are shown in Figures 15, 16, and 17, respectively.

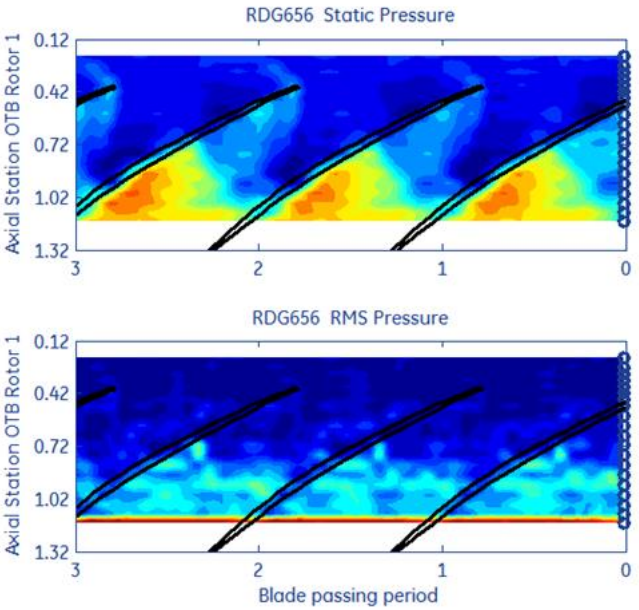

Figure 15. Choke - Kulite data over Rotor 1

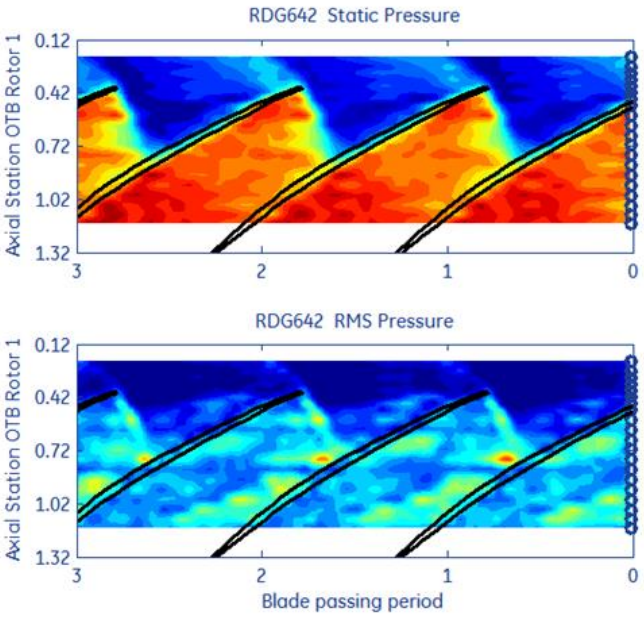

Figure 16. Peak Efficiency - Kulite data over Rotor 1

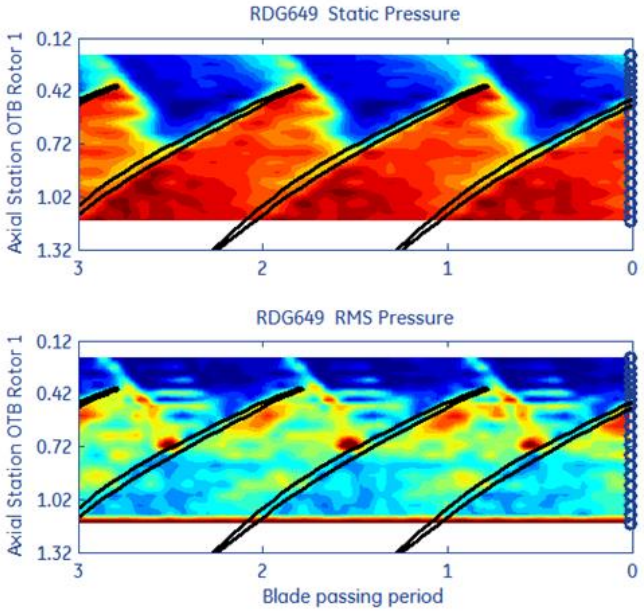

Figure 17. Near-Stall - Kulite data over Rotor 1

The rotor is moving from left to right and the flow is moving from top to bottom. The circles along the right side of the figures show the axial locations of the measurements (refer to Figure 3). In the choked case (Figure 15), the shock, seen in the static pressure contours, is located inside the passage. As the compressor is throttled to peak efficiency (Figure 16), and then to near-stall (Figure 17), the shock moves forward of the rotor leading edge. The RMS pressure shows the tip leakage flow increasing as the rotor is loaded (moving from choke to stall).

CONCLUSIONS

Testing of the first two stages of a highly loaded, advanced GE compressor was performed at NASA Glenn Research Center. The test consisted of 2 configurations; a 1-stage configuration and a 2-stage configuration, in order to separate potential sources of loss. For both configurations, detailed data was taken at 97% Nc, acquiring data from LE instrumentation, wall statics, over the rotor Kulites, and traversing probes.

The results indicated that stage 2 was choking at a mass flow rate which prevented stage 1 from reaching its peak efficiency point, leading to a stage mismatch issue. The mismatch is thought to be due to a loss in the first stage that was unpredicted by design tools. Assessment of

stator 1 leading measurements in both test configurations revealed that the level of performance at this location is unaffected by the presence of the second stage. This suggests that the rotor 2 bow shock interaction with upstream blades is not a significant source of the performance deficit relative to their design intent.

CONTINUING WORK

With the vast amount of high quality data that was taken during this test campaign, there is a large amount of continuing work to be completed beyond what was shown in this report. Analysis of the 100% Nc data, as well as data taken at off-design vane setting angles, is to be performed. Some of the work will be looking in more detail to the unsteady traversing Kulite data, hotwire data, over the rotor Kulite blocks, and 5-Hole probe data. The data set acquired from this test will also be used to validate CFD and help determine how to design accounting for these loss mechanisms.

ACKNOWLEDGEMENTS

This work was supported on a cost shared basis by the NASA Environmentally Responsible Aviation program (ERA) High Pressure Ratio Core Technology and General Electric Aviation. The authors would like to thank Dr. Kenneth Suder of NASA Glenn from the ERA sub-project manager and GE's David Lurie and Andy Breeze-Stringfellow for all their support and technical guidance for this program. We would like to aknowledge John Fabian of Purdue who supported us during this test as the primary NASA researcher. Many thanks to the many test engineers and technicians in the NASA W7 test facility put many long hours into making this test happen

REFERENCES

1. Gibson, M., Graham, A., and Senyitko, R., 2014, "Facility Overview and Subsystem Details High Speed Multistage Compressor Facility Test Cell W7, Building 23," Internal NASA Glenn Publication.
2. Lurie, D., Breeze-Stringfellow, A., Wilson, S., Obear, R., Sohn, K., Shin, H.W., 2014, "Task Order: ERA Advanced Core Compressor Technology Program," NASA Contract # NNC10BA06B Final Report.
3. McCrometer, "Installation Operation & Maintenance Manual, Advanced Differential Pressure Flowmeter Technology", 2010.
4. Strazisar, A.J., 2014, private communication.
5. Cumpsty, N.A., Horlock, J.H., 2005, "Averaging Nonuniform Flow for a Purpose," J. Turbomachinery. 128(1), 120-129.
6. Celestina, M.L., Fabian, J.C., Kulkarni, S., 2012, "NASA Environmentally Responsible Aviation High Overall Pressure Ratio Compressor Research - Pre-Test CFD," 48th AIAA Joint Propulsion Conference, Paper Number 2012-4040.
7. Adamczyk, J., Hansen, J.L., Prahst, P.S.,2007, "A Post Test Analysis of a High-Speed Two-Stage Axial Flow Compressor." ASME GT2007-28057
8. Suder, K.L, "Blockage Development in a Transonic Axial Compressor Rotor", 1997, NASA TM-113115.
9. Larosiliere, L.M., Wood, J.R., Hathaway, M.D., Medd, A.J, Dang, T.Q.,2002, "Aerodynamic Design Study of Advanced Mulitstage Axial Compressor", NASA TP-2002-211568.
10. Coldrick,S., Ivey,P.C., "The Influence of Compressor Aerodynamics on Pressure Probes, Part 1: In Rig Calibrations", 2004, ASME GT2004-53240.
11. Paniagua,G., Denos, R., Oropesa, M., "Thermocouple Probes for Accurate Temperature Measurements in Short Duration Facilities, 2002, ASME GT-2002-30043.
12. Berdanier, R.A., Smith, N.R, Fabian, J.C., Key, N.L.,2014, "Humidity Effects on Experimental Compressor Performance: Corrected Conditions for Real Gases", ASME GT2014-25790.